Research Square

Preprints are preliminary reports that have not undergone peer review.
They should not be considered conclusive, used to inform clinical practice,
or referenced by the media as validated information.

A Deep Learning Framework for Predicting Platinum Drug Sensitivity in Breast Cancer from Histopathological Images: Towards Precision Oncology

Qian Wang
University of Science and Technology of China
Hanlin Wang
University of Science and Technology of China
Ye Feng
University of Science and Technology of China
Cui Zhang
University of Science and Technology of China
Tianzhi Luo
tzluo@ustc.edu.cn

University of Science and Technology of China
Chunguang Miao
Binzhou Medical University

Article

Keywords: Breast cancer, deep learning, platinum drugs, drug sensitivity, predictive model

Posted Date: March 3rd, 2026

DOI: https://doi.org/10.21203/rs.3.rs-8468729/v1

License: This work is licensed under a Creative Commons Attribution 4.0 International License.
Read Full License

Additional Declarations: No competing interests reported.

Abstract

Breast cancer (BC) poses a significant global health challenge due to its high mortality and incidence rates. Although the use of platinum-based drugs in adjuvant chemotherapy has somewhat improved the complete response rate (pCR), the five-year survival rate for metastatic BC remains below 30%. Heterogeneous tumor microenvironments and patient variability lead to divergent drug sensitivities, underscoring the need for predictive tools to optimize treatment. Current organoid-based sensitivity assays face limitations in stability and timeliness, undermining clinical utility. This study analyzed tumor tissues from 63 breast cancer patients through dual approaches: organoid culture for platinum-drug sensitivity grading and histopathological imaging for feature extraction. Texture and nuclear characteristics from primary tumors were quantified using gray-level co-occurrence matrix (GLCM) and OpenCV algorithms. These features were integrated with deep learning models to establish a predictive framework for platinum-drug responsiveness directly from histopathological images. The developed system bypasses time-consuming organoid culture, enabling rapid sensitivity prediction to guide personalized chemotherapy. By correlating morphological patterns with drug response outcomes, this method enhances clinical decision-making for precision oncology, potentially improving survival through early treatment stratification. The approach addresses critical gaps in traditional methods by combining computational pathology with artificial intelligence, offering a scalable solution for real-world BC management.

1. INTRODUCTION

Breast cancer (BC) is one of the most common malignant tumors affecting women globally[1], accounting for approximately 31% of all tumors affecting women. This proportion is projected to increase to 40% by 2040, surpassing lung cancer as the most common malignant tumor globally. In China, BC accounts for 15.59% of all female cancer cases and 7.94% of cancer-related deaths among women. It significantly diminishes patients' quality of life and imposes substantial economic burdens on families and healthcare systems[2]. Currently, surgical removal of tumor tissue remains the primary treatment for BC, often combined with radiotherapy to reduce the risk of local recurrence[3]. Additionally, chemotherapy plays a crucial role as an adjunct therapy, with considerable advancements in its clinical application in recent years[4].

Platinum-based drugs have garnered significant attention due to their high efficacy in tumors with DNA repair deficiencies. Studies have shown that these drugs can significantly improve the pathologic complete response (pCR) [5] in patients with BC. In a clinical trial involving 102 patients with BRCA1 mutations and triple-negative BC, the pCR rate in the cisplatin monotherapy group reached 83%, surpassing rates achieved with other traditional treatment regimens such as CMF (cyclophosphamide-methotrexate-fluorouracil), AT (doxorubicin-docetaxel), AC (doxorubicin-cyclophosphamide), and FAC (fluorouracil-doxorubicin-

cyclophosphamide)[6]. Platinum-based therapies also improve disease-free survival (DFS) and overall survival (OS) in early-stage BC patients receiving neoadjuvant or adjuvant chemotherapy[7] Furthermore, the combination of carboplatin and the PARP (poly ADP-ribose polymerase) inhibitor veliparib has been shown to significantly enhance pCR rates in BC. These findings highlight the potential of platinum-based chemotherapeutics as promising options for adjuvant BC treatment.

Despite the demonstrated efficacy of platinum-based drugs in the neoadjuvant treatment of BC, their sensitivity remains a challenge. Drugs like cisplatin and carboplatin exert their antitumor activity primarily by damaging the molecular structure of tumor cell DNA [8]and activate apoptotic pathways by inducing reactive oxygen species[9]. However, the complex heterogeneity of BC leads to substantial variability in patient responses to these drugs. Some patients exhibit innate resistance to platinum-based therapies, while others develop resistance during chemotherapy. The mechanisms underlying platinum drug resistance in BC are multifaceted. These include reduced intracellular accumulation of the drugs due to altered transport mechanisms[10], increased detoxification through elevated intracellular scavengers such as glutathione, enhanced DNA repair capabilities, and disruptions in apoptotic signaling pathways that enable cancer cells to evade cell death[11,12]. These resistance mechanisms, combined with delays in early BC diagnosis and suboptimal outcomes of postoperative chemotherapy, have limited improvements in survival rates over recent decades. In the era of precision medicine, individualized preclinical research platforms have become essential. Organoids, in particular, are proving to be valuable tools for precision medicine and drug sensitivity screening[13.14]. Organoids can maintain homology with primary tumors over extended periods, providing advantages in high-throughput screening of drug sensitivity[15]. However, organoid-based models face several limitations, including lengthy culture times, low success rates[16,17], and challenges in replicating critical components of the tumor microenvironment, such as stromal cells, blood vessels, and immune system interactions[18]. These limitations hinder the development of effective platinum drug sensitivity screening methods before clinical treatment.

Histopathology has long been considered the gold standard for the clinical diagnosis and prognosis of tumors. By combining hematoxylin and eosin (H&E) staining with immunohistochemical (IHC) analysis of molecular markers, clinicians can achieve more precise companion diagnostics and targeted therapies for tumors[19,20]. The rapid development of digital pathology has further enabled the extraction of clinically relevant information embedded in tumor slides through machine learning and artificial intelligence methods, leveraging advancements in deep learning for image analysis[21]. Whole slide imaging (WSI) has been widely applied in tumor computational diagnosis[22,23], cancer type classification[24,25,26] differentiation of high and low mutation tumors[27], gene mutation identification[28.29.30], patient survival prediction[31,32], DNA methylation pattern detection[33], mitosis[34], quantification of tumor immune infiltration[35], tumor-infiltrating lymphocytes (TIL)[36], and spatial immune cell infiltration. Training deep learning models on the pathological features of BC using WSI offers the potential to predict patient sensitivity to platinum-based drugs. Such approaches could improve the

precision and effectiveness of platinum drug therapies, offering a faster alternative to the lengthy organoid culture process—a field with limited prior exploration.

In this study, we combined deep learning algorithms-assisted pathological analysis and organoid-based platinum drug sensitivity tests to improve the reliability and efficacy of precision medicine. We utilized the HD-YOLO algorithm to identify tumor tissue regions in H&E-stained pathological images of BC tissue samples. Additionally, gray-level co-occurrence matrix (GLCM) and OpenCV algorithms were used to extract features such as tissue texture and nuclear morphology. These tissue features were then correlated with organoid-based platinum drug sensitivity to establish a prediction platform. This platform leverages pathological slides and deep learning techniques, paving the way for more efficient and precise predictions of platinum drug sensitivity in patients with BC.

2. RESULTS AND DISCUSSION

2.1. Construction of a Biobank of BC Organoids

This study successfully established a biobank of living BC organoids by extracting primary tumors from 89 patients with BC, following hospital ethical approval. The tumor samples were divided into two portions: one for organoid construction and the other for histopathological analysis using H&E and IHC staining. Primary tumor cells were isolated from the 89 BC tissues using primary tissue dissociation solution, mixed with matrix gel, and subsequently cultured as organoids (Fig. 1A). Among the samples, 63 BC organoids exhibited successful growth, achieving a success rate of 70.8%. To determine the consistency of the pathological characteristics of the constructed BC organoids with clinical samples, H&E staining was conducted on the 63 BC organoids and their corresponding primary tumor tissues. The analysis revealed that the BC organoids displayed irregular cystic structures and glandular morphologies, closely mirroring the tissue morphology of the original clinical samples (Fig. 2B).

The cell proliferation antigen Ki67, a marker present exclusively in proliferating cells and absent in quiescent phases of the cell cycle[37], is widely regarded as a reliable indicator of BC proliferation activity[38]. The tumor suppressor gene P63, primarily expressed in the myoepithelial cells surrounding the acini and ducts of benign breast lesions, exhibits reduced or absent expression in BC tissues, making it a biomarker for assessing breast tissue health[39]. E-cadherin (E-ca), a calcium-dependent transmembrane glycoprotein, is critical for epithelial cell polarization and differentiation. Dysregulation of E-ca function contributes significantly to BC metastasis and is associated with poorer prognosis and reduced overall survival[40]. This study used IHC to detect the expression of Ki67, P63, and E-ca proteins in 63 BC organoids and their corresponding primary tumor tissues. Notably, P63 and E-ca were downregulated to some extent, whereas Ki67 was upregulated in BC tissues (Fig. 1C). Quantitative analysis of these markers using ImageJ software showed no significant differences in the expression levels of the three proteins between primary tumor tissues and organoids ($p < 0.05$) (Fig. 1D). To determine whether breast cancer organoids can recapitulate the genomic characteristics of their originating primary tumors, we performed whole-exome sequencing (WES) analysis on both the tumors and their derived organoids. By

comparing the WES results of the organoids with their parental tumors, we filtered out variations and excluded polymorphisms. As expected, the organoids exhibited mutation profiles highly consistent with their parental tumors. We analyzed known breast cancer-related mutations, including missense mutations, splice site mutations, frameshift mutations, somatic base substitutions, and copy number variations (CNVs). Most somatic mutations present in the parental tumor tissues were retained in the corresponding breast cancer organoids.The most common breast cancer mutation identified was the PIK3CA missense mutation, which was detected in 2 out of 6 breast cancer organoid lines. Additionally, TP53, a frequently mutated gene in tumors, exhibited missense mutations, nonsense mutations, and frameshift deletions (Frame_Shift_Del) in 3 out of 6 breast cancer organoid lines (Fig. 1E). Regarding somatic base substitution patterns, the most prevalent type of mutation in both breast cancer tumor samples and organoids was C > T/T > C transition mutations (Ti), while the least common type was T > G transversion mutations (Tv) (Fig. 1F).Furthermore, we conducted CNV analyses between the breast cancer organoid lines and their corresponding tumors. The results revealed similar patterns of DNA gains and losses between the UTUC organoid lines and their parental tumors (Fig. 1G). These findings demonstrate that the BC organoids effectively recapitulated and retained the histological and genetic characteristics of their original tumor tissues.

2.2. Classification of Platinum-Based Drug Sensitivity in BC Organoids

To explore the response of clinical organoid samples to different platinum-based drugs, this study tested the drug sensitivity of BC organoids to carboplatin and cisplatin in 57 and 39 cases, respectively. The cultured organoids were seeded into 96-well plates and incubated for 24 hours, followed by treatment with 7 different concentration gradients of cisplatin or carboplatin for each patient-derived organoid. After drug treatment and continued culture for 72 hours, cell viability was assessed for each treatment group, and quantitative analysis was performed using dose-response curves and area under the curve (AUC) (Fig. 2A). Specifically, two different passages of organoid lines were treated with carboplatin and cisplatin at varying concentrations to evaluate their responses. The AUC values for early-passage and late-passage organoids from the same organoid line demonstrated a high degree of consistency, with an R^2 of 0.9033 for carboplatin (Figure S1A) and 0.928 for cisplatin (Figure S1B). The results revealed substantial variability in drug sensitivity among organoids derived from different patients with BC. Significant differences were observed in the response to carboplatin (Fig. 2B, 2D) and cisplatin (Fig. 2C, 2E). Dose-response curves and AUC analysis highlighted that while some organoids were resistant to carboplatin, they exhibited partial sensitivity or full sensitivity to cisplatin (Figures S1C). Based on the drug dose-response curves and AUC quantification results, this study further categorized the BC organoids according to their sensitivity to carboplatin, resulting in a resistant group of 19 cases, an intermediate group of 19 cases, and a sensitive group of 19 cases (Fig. 2F). Similarly, the BC organoids were categorized based on their sensitivity to cisplatin, with a resistant group of 13 cases, an intermediate group of 13 cases, and a sensitive group of 13 cases (Fig. 2G). Notably, organoids from the same patient displayed differing sensitivities to carboplatin and cisplatin (Figure S1C), underscoring the

heterogeneity in drug responses. These categorized groups formed the basis for constructing a predictive model of platinum drug sensitivity using BC organoids.

2.3. Tumor Heterogeneity and Its Pathological Characteristics

The tumor stroma, immune cells, nutrients in the microenvironment, DNA damage, and epigenome, among other intrinsic factors, together constitute the heterogeneity of tumors (Fig. 3A-H). These molecular characteristics provide key information regarding tumor origin, progression, drug sensitivity, and expected prognosis[41]. Single-cell genomics (such as single-cell RNA sequencing), metabolomics, and proteomics technologies allow for the genetic barcoding of individual cells within tissues, enabling the dissection of the heterogeneity of each single cell in the tumor microenvironment[42]. Additionally, GLCM texture analysis plays a significant role in the diagnosis and classification of BC. At a smaller scale, it can extract microscopic texture features of tumor cells, such as the texture of the nuclei and the spatial relationships between cells[43]. At a larger scale, it can extract macroscopic texture features of tumor tissues, such as the edges, shapes, and internal structures of tumors. These multi-scale texture features can reflect the structural and characteristic differences at various levels of tumor tissues, providing more comprehensive tumor information[44], which helps to more accurately predict the sensitivity of BC to platinum-based therapeutic agents.

The area and perimeter of BC cell nuclei are closely related to drug sensitivity[45](Fig. 3I). Studies indicate that approximately 40% of patients with larger nuclear areas exhibit resistance to certain chemotherapy drugs[46] The perimeter of the nucleus, which reflects the complexity of its shape, is another critical factor. Nuclei with longer perimeters are often linked to increased tumor aggressiveness, which can negatively impact drug sensitivity. Notably, about 35% of patients with longer nuclear perimeters show poor responses to targeted therapy[46]. Roundness measures the extent to which a nucleus approximates a circular shape, while eccentricity quantifies how elongated or flattened the nucleus is. The aspect ratio provides further details about the nucleus's shape by comparing its length to its width. The nuclear-cytoplasmic ratio reflects the proportional relationship between the nucleus and the surrounding cytoplasm. These nuclear characteristics are strongly linked to drug sensitivity. Tumor cells with lower roundness, higher eccentricity, larger aspect ratios, and elevated nuclear-cytoplasmic ratios often exhibit reduced sensitivity to endocrine therapy drugs[47]. Classifying BC based on nuclear characteristics can provide a basis for predicting drug sensitivity.

2.4. Tumor cell region recognition and feature extraction based on deep learning for pathological tissue sections

The effectiveness of cancer chemotherapy often suffers due to inappropriate drug selection, with conventional "randomized" or "standardized" approaches failing to account for the diverse phenotypes and genetic backgrounds of tumors. This variability leads to differing tumor sensitivities and tolerances to chemotherapy drugs, rendering these traditional methods suboptimal for many patients. Most cancer

cases are not suitable for this "uniform" or "standardized" chemotherapy. Therefore, developing a clinically practical drug selection system is as crucial as discovering new drugs. Introducing mathematical and computational systems to analyze tumor characteristics and optimize drug selection can significantly improve treatment outcomes[48]. For example, using gene expression features and drug sensitivity data from the Cancer Cell Line Encyclopedia (CCLE) to construct a predictor based on Support Vector Machine (SVM) and recursive feature selection tools can effectively predict drug sensitivity in tumor patients[49].

This study employs the YOLO-V5 algorithm, a lightweight convolutional neural network (CNN) model, to design and implement a deep learning-based approach for identifying tumor regions in BC pathological tissue images and predicting sensitivity to platinum-based drugs. The YOLO-V5 model comprises four key components: input, backbone, neck, and head (Fig. 4A). This model offers a fast detection speed, high accuracy, and flexibility. The input module preprocesses pathological images before analysis, while the backbone network extracts detailed image features using the BottleNeckCSP structure, integrating CSPNet architecture, convolutional layers, and residual modules. The neck module fuses multi-scale features using the Spatial Pyramid Pooling (SPP) structure, and the head module produces the final detection results, including tumor classifications and object locations.

First, the pathological images of BC tissues were divided into three groups: training set (60%), test set (30%), and validation set (10%). Expert pathologists manually annotated the images in the training and test sets, marking tumor regions in red and non-tumor regions in green. These annotations were used to train and optimize the recognition model, with the best-performing version saved for evaluation on the validation set. The test results were subsequently verified by professional pathologists to ensure accuracy (Fig. 4B). Based on the identified tumor regions, pathological feature information (including texture features, contrast, roughness, heterogeneity, homogeneity, and entropy) and nuclear morphological features (including nuclear perimeter, area, roundness, and eccentricity) were extracted using GLCM and OpenCV (Fig. 4C). Statistical revealed a negative correlation between the nuclear area of tumor cells in the carboplatin group and drug sensitivity (Fig. 4D, S2A). This may be attributed to the heightened proliferative activity of tumor cells with larger nuclear areas, which reduces drug sensitivity. Conversely, the texture feature of pathological tissue, specifically contrast, showed a positive correlation with drug sensitivity. This suggests that the contrast feature captures changes in tumor cells and their microenvironment, emphasizing the critical role of the tumor microenvironment in determining tumor prognosis. For the cisplatin group, a negative correlation was observed between cell roundness and organoid drug sensitivity (Fig. 4E, S2B). Increased irregularity in cell shapes may reflect altered gene expression patterns and signaling pathways, which impact drug efficacy. Conversely, the aspect ratio was positively correlated with organoid drug sensitivity, implying that highly proliferative cells may deploy intracellular mechanisms to resist cytotoxic effects, leading to poorer outcomes. The texture feature angular second moment (ASM) was found to reflect tissue roughness, with higher roughness observed in cisplatin-resistant pathological tissues compared to sensitive tissues. This increased roughness is likely due to enhanced cellular heterogeneity, which adversely affects treatment outcomes.

In summary, the model constructed in this study demonstrates a strong correlation between pathological texture features, nuclear morphological characteristics, and drug sensitivity in BC organoids. These findings provide a theoretical foundation for developing a predictive platform for drug sensitivity in clinical settings.

2.5. Drug response prediction model based on drug sensitivity of BC organoids

Based on the histopathological images of 63 clinical samples from patients with BC and the corresponding drug sensitivity of organoids through deep learning, this study further constructed a model to directly predict sensitivity to platinum-based drugs (Fig. 5A). The model's performance was evaluated by comparing the predicted sensitivity of each tissue to platinum-based drugs with the actual sensitivity in the test dataset samples. The drug sensitivity data was divided into three parts: training set (60%), test set (30%), and validation set (10%). Predicted outcomes of 0, 0.5, and 1 corresponded to sensitive, intermediate, and resistant drug sensitivity groups, respectively (Fig. 5B). To further improve the model's predictive accuracy, various optimization methods were employed. Specifically, the multilayer perceptron algorithm, widely used in deep learning, was selected, along with the Adam optimizer. The Adam optimizer combines the advantages of adaptive learning rates and momentum, allowing for automatic adjustment of the learning rate during training, accelerating the model's convergence speed while avoiding local optima. The ReLU function was used as the model's activation function, achieving advantages such as simple computation and fast convergence, effectively avoiding the gradient vanishing problem. To prevent overfitting, early stopping was applied, halting training when no further improvements in model performance were observed. These optimization techniques collectively enhanced the model's capability to predict drug sensitivity in patients with BC.

The test results demonstrated that using texture features alone provided moderate predictive accuracy for drug sensitivity in BC organoids. The area under the receiver operating characteristic (ROC) curve (AUC) reached 0.86 for carboplatin (Figs. 5C) and 0.64 for cisplatin (Figs. 5E), indicating that the predictive accuracy using texture features alone was relatively limited. Similarly, nuclear features alone offered valuable predictive information, yielding AUC values above 0.6 for both carboplatin and cisplatin. However, relying solely on nuclear features also proved inadequate in capturing the comprehensive tumor characteristics (Figs. 5C and 5E). Texture features representing the macroscopic structure and heterogeneity of tumors, and nuclear features reflecting the microscopic properties of tumor cells, were integrated into the model. This combination resulted in a notable improvement in the prediction of cisplatin sensitivity, although it caused a slight reduction in predictive accuracy for carboplatin. Further refinement of the model involved selecting features most relevant to drug sensitivity groupings. This approach significantly improved predictions for both drugs, achieving the highest AUC values: 0.95 for carboplatin (Figs. 5D) and 0.93 for cisplatin (Figs. 5F). These findings underscore the complementarity of texture and nuclear features in predicting drug sensitivity.

3. MATERIALS AND METHODS

3.1. Main Experimental Materials

Carboplatin and cisplatin were purchased from MCE (New Jersey, USA). The CellTiter-Glo cell viability assay kit was purchased from Promega (Wisconsin, USA). DMEM/F-12 basal medium was purchased from Thermo (Massachusetts, USA). Tissue lysis buffer, red blood cell lysis buffer, matrix gel, and organoid culture medium were provided by Luohua Biotechnology (Hefei, China). Ki67 monoclonal antibody, P63 monoclonal antibody, E-cadherin monoclonal antibody, and HRP-conjugated rabbit and mouse secondary antibodies were purchased from Dako (Copenhagen, Denmark).

3.2. Human Tissue Specimens

This study was reviewed and approved by the Ethics Committees of the First Affiliated Hospital of University of Science and Technology of China and the First People's Hospital of Bengbu. All participants provided informed consent and voluntarily participated in the study by signing informed consent forms, ensuring compliance with ethical standards and safeguarding participants' rights. Human BC samples were obtained from the hospital and confirmed by two independent pathologists using H&E staining and IHC staining. Each tumor specimen was divided into two portions: one for histopathological analysis and the other for organoid culture processing.

3.3. Isolation and Culture of Tumor Organoids

BC tissue was washed with DMEM/F12 under sterile conditions, and all dead cells and non-epithelial tissues (such as muscle, fat, or capillaries) were removed as much as possible using sterile tweezers. The tissue was cut into pieces approximately the size of a rice grain in a culture dish and transferred to a 15 mL centrifuge tube. The tissue fragments were resuspended in pre-warmed primary tissue dissociation solution and digested in a temperature-controlled mixer at 37°C and 200 rpm for 15–20 minutes. To terminate the digestion process, 200 μL of fetal bovine serum was gently mixed into the tissue suspension. The suspension was then filtered through a 70 μm cell strainer, and the filtrate was collected. The filtrate was centrifuged at 300 g for 3 minutes, after which the supernatant was discarded, retaining the pellet. The pellet was treated with Red Blood Cell Lysis Solution to remove red blood cells, followed by three washes with DMEM/F12 medium. One milliliter of organoid culture medium was added to the pellet for resuspension, and the cell count was performed. A total of 2 × 105 primary BC cells were mixed with matrix gel at a volume ratio of 1:4. The mixture was evenly seeded in a 24-well plate, creating 3–4 matrix gel beads per well, with each bead containing 10 μL. The plate was inverted and incubated at 37°C for 40 minutes to allow the matrix gel to solidify. After solidification, 400 μL of organoid culture medium was added to each well, and the cultures were maintained in a 37°C, 5% CO_2 incubator.

3.4. H&E and IHC Staining of Tissues and Organoids

Tumor tissues or organoids embedded in 5 mm paraffin were processed for H&E and IHC staining. All sections underwent deparaffinization and rehydration. For H&E staining, sections were stained with hematoxylin and eosin. For IHC, sections were subjected to antigen retrieval using sodium EDTA and blocked with 20% goat serum for 30 minutes to reduce background. The primary antibody was applied

and incubated overnight at 4°C. After washing, sections were incubated with an HRP-conjugated secondary antibody for 30 minutes, followed by color development using 3,3'-diaminobenzidine (DAB), which produced a brown stain at antigen-antibody interaction sites. Images were captured using a microscope and camera. For quantification, five randomly selected areas from each section were photographed at 20× magnification. An experienced pathologist evaluated the positive staining scores or densities of stained cells.

3.5. Drug Screening and Cell Viability Assay

Organoids were resuspended in matrix gel and seeded as suspensions in a 96-well plate, with each well containing 5 μL of matrix gel and approximately 500 cells. After one day of cell culture, the medium was replaced with fresh medium containing varying concentrations of carboplatin or cisplatin. The organoids were then cultured for an additional three days. Following drug treatment, cell viability was assessed using the CellTiter-Glo cell viability assay kit. The dose-response curve was generated using GraphPad Prism 9.0 and fitted with a three-parameter logistic regression model, employing a variable slope and constraints set at 100% and 0% viability. The AUC was calculated from the raw experimental data and normalized by dividing the AUC by the total maximum area under the curve, corresponding to 0%–100% survival within the tested drug concentration range.

3.6. Drug Sensitivity Prediction Model

Organoids derived from 63 clinical BC tissues were categorized into three groups based on drug sensitivity test results: resistant group (top 33% AUC), sensitive group (bottom 33% AUC), and intermediate group (middle 34% AUC). These groups were used as the training dataset. The pathological tissue differential features between sensitive and non-sensitive groups (including resistant and intermediate groups) were used as input to construct the drug sensitivity prediction model. A multilayer perceptron (MLP) algorithm was used as a classifier, and model testing was conducted to select the best predictive feature set for optimal predictive performance. Finally, the predictive performance of the model was visualized through the receiver operating characteristic (ROC) curve. All procedures were executed using default parameters.

3.7. Quantification and Statistical Analysis

All summarized data are presented as mean ± standard deviation, or as representative images derived from at least three independent experiments. Statistical analyses were performed in R (v 4.0.2), Python (v 3.9.7), and GraphPad Prism (version 9.0). The sample size (n) values used for statistical analysis are indicated in the relevant figures and supplementary figures. Individual data points are represented graphically or can be found in the source data. Differences between two groups were tested using Student's two-tailed unpaired t-test or one-way ANOVA. When using t-tests, we assumed that the variances between different groups were normally distributed and homogeneously distributed. The significance level for all tests was set at $p < 0.05$.

4. CONCLUSION

This study successfully constructed an advanced model to predict the sensitivity of BC to platinum-based chemotherapy, aiming to provide a scientific basis for personalized treatment by directly predicting patients' sensitivity to platinum-based chemotherapy using clinical histopathological images of clinical BC samples. Initially, We established BC organoids from the clinical tissues of 61 patients with BC and categorized them into sensitive, intermediate, and resistant groups based on their sensitivity to carboplatin and cisplatin. Texture features (using GLCM) and nuclear features (using OpenCV algorithm) were obtained from histopathological images of the different groups. These features were integrated with deep learning algorithms to analyze the correlation between pathological characteristics and sensitivity to platinum drugs. The resulting model demonstrated the ability to predict drug sensitivity based on clinical histopathological images of BC samples (Fig. 6), providing strong support and guidance for personalized treatment of BC.

Next, we conducted an in-depth analysis of the complex relationship between texture features in histopathological images and tumors, as well as the close association between nuclear features and BC. GLCM texture features were shown to effectively capture tumor heterogeneity, serving as potential biomarkers for BC classification and prognostic prediction. These findings underline their potential clinical significance. Similarly, nuclear features extracted with the OpenCV algorithm were demonstrated to be closely linked to BC prognosis and had a significant impact on the drug sensitivity of BC organoids. The study emphasized meticulous data collection and processing to ensure the quality and diversity of the histopathological images used. Mature algorithms were utilized to extract both GLCM texture features and nuclear features, which were then seamlessly integrated into the predictive model. The deep learning framework adopted for this study combined Convolutional Neural Networks (CNN) and Multi-Layer Perceptrons (MLP), leveraging optimization algorithms and various strategies to enhance the model's performance and generalizability. In the experimental and result analysis, a control group was established, and suitable experimental indicators and evaluation methods were selected to rigorously assess the model. Comparative analyses were conducted to evaluate the impact of different features on prediction results and benchmark the framework against existing methods. These analyses confirmed the effectiveness and superiority of the proposed deep learning framework, which integrates texture and nuclear features, in predicting BC patients' sensitivity to platinum-based drugs, highlighting the significant potential of this approach for clinical applications.

In conclusion, the deep learning framework constructed in this study provides new ideas and methods for the personalized treatment of BC, demonstrating significant clinical application potential. However, this study also has some limitations, such as a relatively small sample size and lack of multi-center validation. Future research could further expand the sample size and conduct multi-center validation to improve the reliability and generalizability of the model. Additionally, we can explore more feature extraction methods and deep learning algorithms to continuously optimize the model, providing more accurate and efficient predictive tools for the treatment of BC and advancing personalized medicine.

Declarations

ACKNOWLEDGEMENTS

This work was financially supported by the Science Project of Anhui Province in China (Grant Nos. 202203a07020006), the Key R&D Program of Shandong Province, China (Grant No. 2023CXPT012), Anhui Provincial Innovation Platform of Major Science and Technology Project (202305a12020024), the Scientific Research Major Project of Anhui Provincial Education Department (2024AH040142) and Anhui Provincial Natural Science Foundation of China Youth Project (Class C)grant no. 2508085QH284. We sincerely thank Anhui Luohua Biotechnology Co., Ltd. for their invaluable technical support throughout this research.

Declaration of interests

The authors declare that they have no known competing financial interests or personal relationships that could have appeared to influence the work reported in this paper.

The authors declare the following financial interests/personal relationships which may be considered as potential competing interests:

Author Statement

We declare that this manuscript is original, has not been published before and is notcurrently being considered for publication elsewhere.

We confirm that the manuscript has been read and approved by all named authors andthat there are no other persons who satisfied the criteria for authorship but are not listedWe further confirm that the order of authors listed in the manuscript has been approvecby all ofus.

We understand that the Corresponding Author is the sole contact for the Editoriaprocess. She is responsible for communicating with the other authors about progresssubmissions of revisions, and final approval of proofs.

All authors as follows:

Qian Wang(First Author) responsible for proposing hypotheses and reviewing drafts

Hanlin Wang responsible for formal analysis of model construction and validation

Ye Feng responsible for collecting and organizing breast cancer pathology image data

Cui Zhang responsible for design and code implementation of YOLO-V5/CNN-MLP fusion method, drafting initial paper

Tianzhi Luo(Corresponding Author) and Chunguang Miao(Corresponding Author) prepared securing research funding, coordinating resources, and revising/finalizing papers

All authors reviewed the manuscript

Ethics statements

This retrospective study was approved by the Ethics Committee of Bengbu First People's Hospital and the methods were carried out in accordance with the approved quidelines. Ethics Approval Number is BBYY2023082. Althe patients have been informed and siqned informed consent before theexperiments

References

1. Arnold M., Morgan E., Rumgay H., et al. (2022). Current and future burden of breast cancer: Global statistics for 2020 and 2040. *Breast (Edinburgh, Scotland)* **66**:15-23. DOI:10.1016/j.breast.2022.08.010
2. Sun K., Zhang B., Lei S., et al. (2024). Incidence, mortality, and disability-adjusted life years of female breast cancer in China, 2022. *Chinese medical journal* **137**:2429-2436. DOI:10.1097/cm9.0000000000003278
3. Jacobs A. T., Martinez Castaneda-Cruz D., Rose M. M., et al. (2022). Targeted therapy for breast cancer: An overview of drug classes and outcomes. *Biochemical pharmacology* **204**:115209. DOI:10.1016/j.bcp.2022.115209
4. Ye F., Dewanjee S., Li Y., et al. (2023). Advancements in clinical aspects of targeted therapy and immunotherapy in breast cancer. *Molecular cancer* **22**:105. DOI:10.1186/s12943-023-01805-y
5. Cortazar P., Zhang L., Untch M., et al. (2014). Pathological complete response and long-term clinical benefit in breast cancer: the CTNeoBC pooled analysis. *Lancet (London, England)* **384**:164-172. DOI:10.1016/s0140-6736(13)62422-8
6. Byrski T., Gronwald J., Huzarski T., et al. (2010). Pathologic complete response rates in young women with BRCA1-positive breast cancers after neoadjuvant chemotherapy. *Journal of clinical oncology : official journal of the American Society of Clinical Oncology* **28**:375-379. DOI:10.1200/jco.2008.20.7019
7. Mason S. R., Willson M. L., Egger S. J., et al. (2023). Platinum-based chemotherapy for early triple-negative breast cancer. *The Cochrane database of systematic reviews* **9**:Cd014805. DOI:10.1002/14651858.CD014805.pub2
8. Tchounwou P. B., Dasari S., Noubissi F. K., et al. (2021). Advances in Our Understanding of the Molecular Mechanisms of Action of Cisplatin in Cancer Therapy. *Journal of experimental pharmacology* **13**:303-328. DOI:10.2147/jep.S267383
9. Fumarola S., Cecati M., Sartini D., et al. (2020). Bladder Cancer Chemosensitivity is Affected by Paraoxonase-2 Expression. *Antioxidants (Basel, Switzerland)* **9**. DOI:10.3390/antiox9020175
10. Galluzzi L., Vitale I., Michels J., et al. (2014). Systems biology of cisplatin resistance: past, present and future. *Cell death & disease* **5**:e1257. DOI:10.1038/cddis.2013.428

11. Köberle B., Tomicic M. T., Usanova S., et al. (2010). Cisplatin resistance: preclinical findings and clinical implications. *Biochimica et biophysica acta* **1806**:172-182. DOI:10.1016/j.bbcan.2010.07.004
12. Amable L. (2016). Cisplatin resistance and opportunities for precision medicine. *Pharmacological research* **106**:27-36. DOI:10.1016/j.phrs.2016.01.001
13. Aboulkheyr Es H., Montazeri L., Aref A. R., et al. (2018). Personalized Cancer Medicine: An Organoid Approach. *Trends in biotechnology* **36**:358-371. DOI:10.1016/j.tibtech.2017.12.005
14. Jin M. Z., Han R. R., Qiu G. Z., et al. (2018). Organoids: An intermediate modeling platform in precision oncology. *Cancer letters* **414**:174-180. DOI:10.1016/j.canlet.2017.11.021
15. Xu H., Jiao D., Liu A., et al. (2022). Tumor organoids: applications in cancer modeling and potentials in precision medicine. *Journal of hematology & oncology* **15**:58. DOI:10.1186/s13045-022-01278-4
16. Lee S. H., Hu W., Matulay J. T., et al. (2018). Tumor Evolution and Drug Response in Patient-Derived Organoid Models of Bladder Cancer. *Cell* **173**:515-528.e517. DOI:10.1016/j.cell.2018.03.017
17. Maru Y., Tanaka N., Itami M., et al. (2019). Efficient use of patient-derived organoids as a preclinical model for gynecologic tumors. *Gynecologic oncology* **154**:189-198. DOI:10.1016/j.ygyno.2019.05.005
18. Huang Y., Huang Z., Tang Z., et al. (2021). Research Progress, Challenges, and Breakthroughs of Organoids as Disease Models. *Frontiers in cell and developmental biology* **9**:740574. DOI:10.3389/fcell.2021.740574
19. Curtis C., Shah S. P., Chin S. F., et al. (2012). The genomic and transcriptomic architecture of 2,000 breast tumours reveals novel subgroups. *Nature* **486**:346-352. DOI:10.1038/nature10983
20. Doroshow D. B. and Doroshow J. H. (2020). Genomics and the History of Precision Oncology. *Surgical oncology clinics of North America* **29**:35-49. DOI:10.1016/j.soc.2019.08.003
21. Rosenthal J., Carelli R., Omar M., et al. (2022). Building Tools for Machine Learning and Artificial Intelligence in Cancer Research: Best Practices and a Case Study with the PathML Toolkit for Computational Pathology. *Molecular cancer research : MCR* **20**:202-206. DOI:10.1158/1541-7786.Mcr-21-0665
22. Ström P., Kartasalo K., Olsson H., et al. (2020). Artificial intelligence for diagnosis and grading of prostate cancer in biopsies: a population-based, diagnostic study. *The Lancet. Oncology* **21**:222-232. DOI:10.1016/s1470-2045(19)30738-7
23. Fu Y., Jung A. W., Torne R. V., et al. (2020). Pan-cancer computational histopathology reveals mutations, tumor composition and prognosis. *Nature cancer* **1**:800-810. DOI:10.1038/s43018-020-0085-8
24. Coudray N., Ocampo P. S., Sakellaropoulos T., et al. (2018). Classification and mutation prediction from non-small cell lung cancer histopathology images using deep learning. *Nature medicine* **24**:1559-1567. DOI:10.1038/s41591-018-0177-5
25. Swiderska-Chadaj Z., Pinckaers H., van Rijthoven M., et al. (2019). Learning to detect lymphocytes in immunohistochemistry with deep learning. *Medical image analysis* **58**:101547.

DOI:10.1016/j.media.2019.101547

26. Yu K. H., Wang F., Berry G. J., et al. (2020). Classifying non-small cell lung cancer types and transcriptomic subtypes using convolutional neural networks. *Journal of the American Medical Informatics Association : JAMIA* **27**:757-769. DOI:10.1093/jamia/ocz230
27. Xu H., Clemenceau J. R., Park S., et al. (2022). Spatial heterogeneity and organization of tumor mutation burden with immune infiltrates within tumors based on whole slide images correlated with patient survival in bladder cancer. *Journal of pathology informatics* **13**:100105. DOI:10.1016/j.jpi.2022.100105
28. Kather J. N., Heij L. R., Grabsch H. I., et al. (2020). Pan-cancer image-based detection of clinically actionable genetic alterations. *Nature cancer* **1**:789-799. DOI:10.1038/s43018-020-0087-6
29. Kather J. N., Pearson A. T., Halama N., et al. (2019). Deep learning can predict microsatellite instability directly from histology in gastrointestinal cancer. *Nature medicine* **25**:1054-1056. DOI:10.1038/s41591-019-0462-y
30. Ghaffari Laleh N., Muti H. S., Loeffler C. M. L., et al. (2022). Benchmarking weakly-supervised deep learning pipelines for whole slide classification in computational pathology. *Medical image analysis* **79**:102474. DOI:10.1016/j.media.2022.102474
31. Mobadersany P., Yousefi S., Amgad M., et al. (2018). Predicting cancer outcomes from histology and genomics using convolutional networks. *Proceedings of the National Academy of Sciences of the United States of America* **115**:E2970-e2979. DOI:10.1073/pnas.1717139115
32. Cheng J., Zhang J., Han Y., et al. (2017). Integrative Analysis of Histopathological Images and Genomic Data Predicts Clear Cell Renal Cell Carcinoma Prognosis. *Cancer research* **77**:e91-e100. DOI:10.1158/0008-5472.Can-17-0313
33. Zheng H., Momeni A., Cedoz P. L., et al. (2020). Whole slide images reflect DNA methylation patterns of human tumors. *NPJ genomic medicine* **5**:11. DOI:10.1038/s41525-020-0120-9
34. Wang H., Cruz-Roa A., Basavanhally A., et al. (2014). Mitosis detection in breast cancer pathology images by combining handcrafted and convolutional neural network features. *Journal of medical imaging (Bellingham, Wash.)* **1**:034003. DOI:10.1117/1.Jmi.1.3.034003
35. Turkki R., Linder N., Kovanen P. E., et al. (2016). Antibody-supervised deep learning for quantification of tumor-infiltrating immune cells in hematoxylin and eosin stained breast cancer samples. *Journal of pathology informatics* **7**:38. DOI:10.4103/2153-3539.189703
36. Saltz J., Gupta R., Hou L., et al. (2018). Spatial Organization and Molecular Correlation of Tumor-Infiltrating Lymphocytes Using Deep Learning on Pathology Images. *Cell reports* **23**:181-193.e187. DOI:10.1016/j.celrep.2018.03.086
37. Page D. B., Broeckx G., Jahangir C. A., et al. (2023). Spatial analyses of immune cell infiltration in cancer: current methods and future directions: A report of the International Immuno-Oncology Biomarker Working Group on Breast Cancer. *The Journal of pathology* **260**:514-532. DOI:10.1002/path.6165

38. Louis D. M., Nair L. M., Vallonthaiel A. G., et al. (2023). Ki 67: a Promising Prognostic Marker in Early Breast Cancer-a Review Article. *Indian journal of surgical oncology* **14**:122-127. DOI:10.1007/s13193-022-01631-6
39. Lashen A. G., Toss M. S., Ghannam S. F., et al. (2023). Expression, assessment and significance of Ki67 expression in breast cancer: an update. *Journal of clinical pathology* **76**:357-364. DOI:10.1136/jcp-2022-208731
40. Alkhayyat R., Abbas A., Quinn C. M., et al. (2024). Tumour 63 protein (p63) in breast pathology: biology, immunohistochemistry, diagnostic applications, and pitfalls. *Histopathology* **84**:723-741. DOI:10.1111/his.15101
41. Corso G., Figueiredo J., De Angelis S. P., et al. (2020). E-cadherin deregulation in breast cancer. *Journal of cellular and molecular medicine* **24**:5930-5936. DOI:10.1111/jcmm.15140
42. Pasha N. and Turner N. C. (2021). Understanding and overcoming tumor heterogeneity in metastatic breast cancer treatment. *Nature cancer* **2**:680-692. DOI:10.1038/s43018-021-00229-1
43. Perkel J. M. J. N. (2021). Single-cell analysis enters the multiomics age. **595**:614-616.
44. Huisman A., Ploeger L. S., Dullens H. F., et al. (2005). Development of 3D chromatin texture analysis using confocal laser scanning microscopy. *Cellular oncology : the official journal of the International Society for Cellular Oncology* **27**:335-345. DOI:10.1155/2005/494605
45. Alibabaei S., Rahmani M., Tahmasbi M., et al. (2023). Evaluating the Gray Level Co-Occurrence Matrix-Based Texture Features of Magnetic Resonance Images for Glioblastoma Multiform Patients' Treatment Response Assessment. *Journal of medical signals and sensors* **13**:261-271. DOI:10.4103/jmss.jmss_50_22
46. Samaratunga H., Delahunt B., Yaxley J. W., et al. (2021). Intraductal Carcinoma of the Prostate: Extreme Nuclear Size Is Not a Diagnostic Parameter. *The American journal of surgical pathology* **45**:1527-1533. DOI:10.1097/pas.0000000000001776
47. Huang P., Zhou X., He P., et al. (2023). Interpretable laryngeal tumor grading of histopathological images via depth domain adaptive network with integration gradient CAM and priori experience-guided attention. *Computers in biology and medicine* **154**:106447. DOI:10.1016/j.compbiomed.2022.106447
48. Lu D. Y., Chen X. L. and Ding J. (2006). Individualized cancer chemotherapy integrating drug sensitivity tests, pathological profile analysis and computational coordination - an effective strategy to improve clinical treatment. *Medical hypotheses* **66**:45-51. DOI:10.1016/j.mehy.2005.07.023
49. Dong Z., Zhang N., Li C., et al. (2015). Anticancer drug sensitivity prediction in cell lines from baseline gene expression through recursive feature selection. *BMC cancer* **15**:489. DOI:10.1186/s12885-015-1492-6

Figures

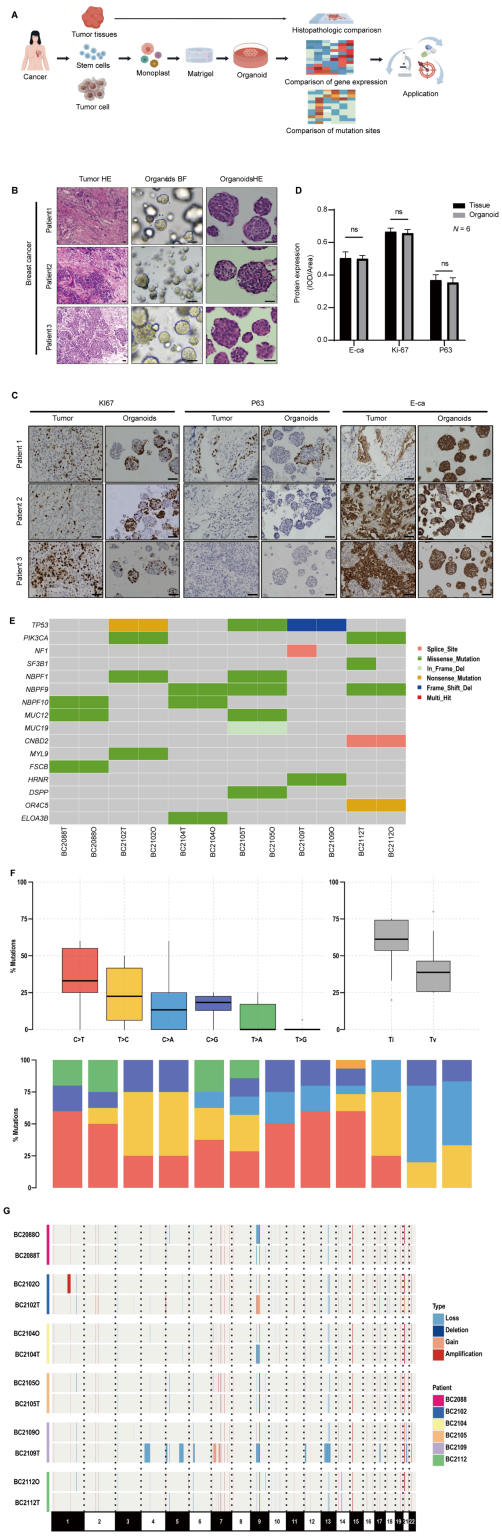


Figure 1

Construction of the BC organoid sample library. (A) Organoid construction process. (B) H&E staining of tumor tissue and organoids. (C) IHC staining of tumor tissue and organoids. (D) The protein expression levels of the three cellular markers E-cadherin, Ki-67, and P63 in tissue and organoid samples are presented. Scale bar: 50 micrometers. (E) Recurrent mutations identified in the parental tumor and corresponding organoid lines by WES. Displayed are the top 20 mutated genes observed in the data. (F)

Percentage of the six types of SNVs, averaged across all samples. Proportions of exonic variants across the samples. The six types of SNVs are represented. (G) Concordance of mutations detected in the parental tumor and corresponding organoid line.

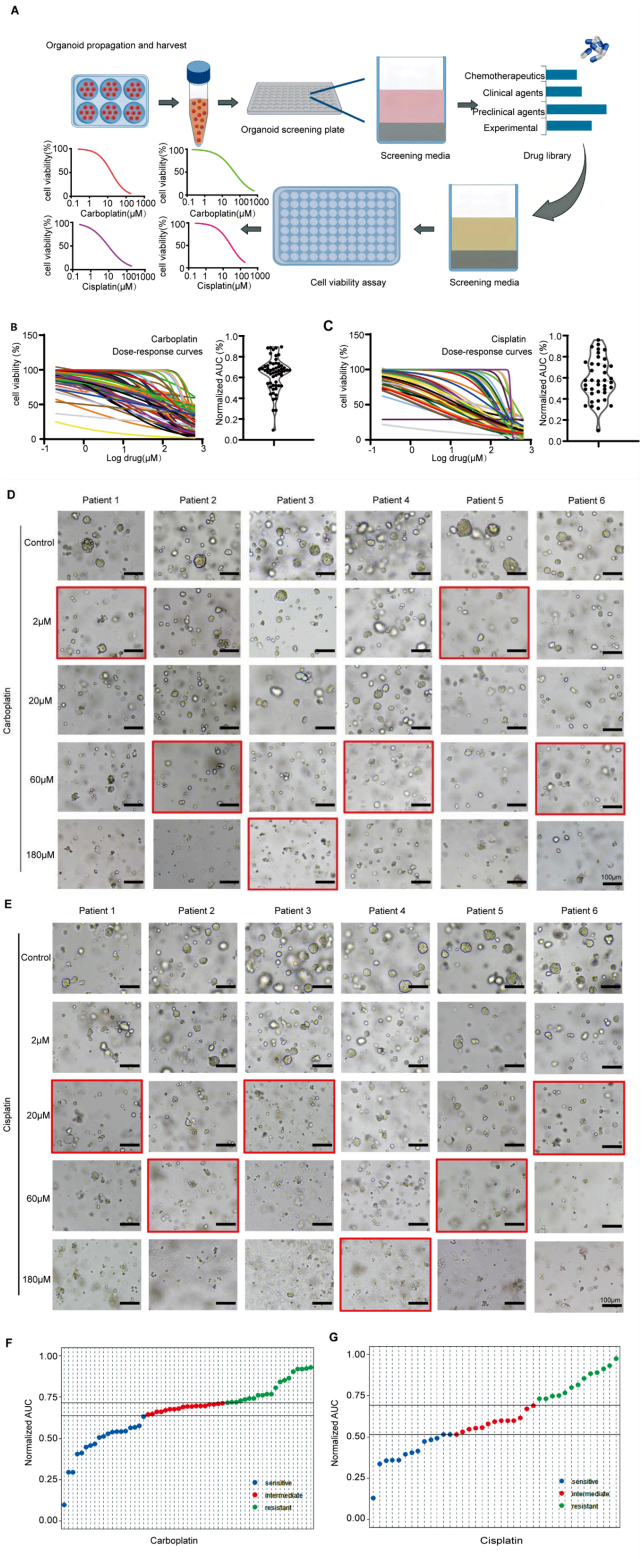


Figure 2

Responses of breast cancer organoids to chemotherapy drugs in vitro. (A) Experimental design for the sensitivity testing of clinical chemotherapy drugs on breast cancer organoids. (B) and (C) Summary of

the drug sensitivity responses of 63 breast cancer organoids to carboplatin and cisplatin, presented in the form of dose-response curves, with AUC calculated from the original dose-response data and displayed using violin plots. (D) and (E) These panels analyze the impact of different concentration gradient chemotherapy drugs on organoid viability based on organoid survival status, with red squares representing organoid death. Scale bar: 100 micrometers. (F) and (G) Classification of breast cancer organoids into three groups based on drug sensitivity test results: sensitive group, intermediate group, and resistant group, (F) carboplatin, (G) cisplatin.

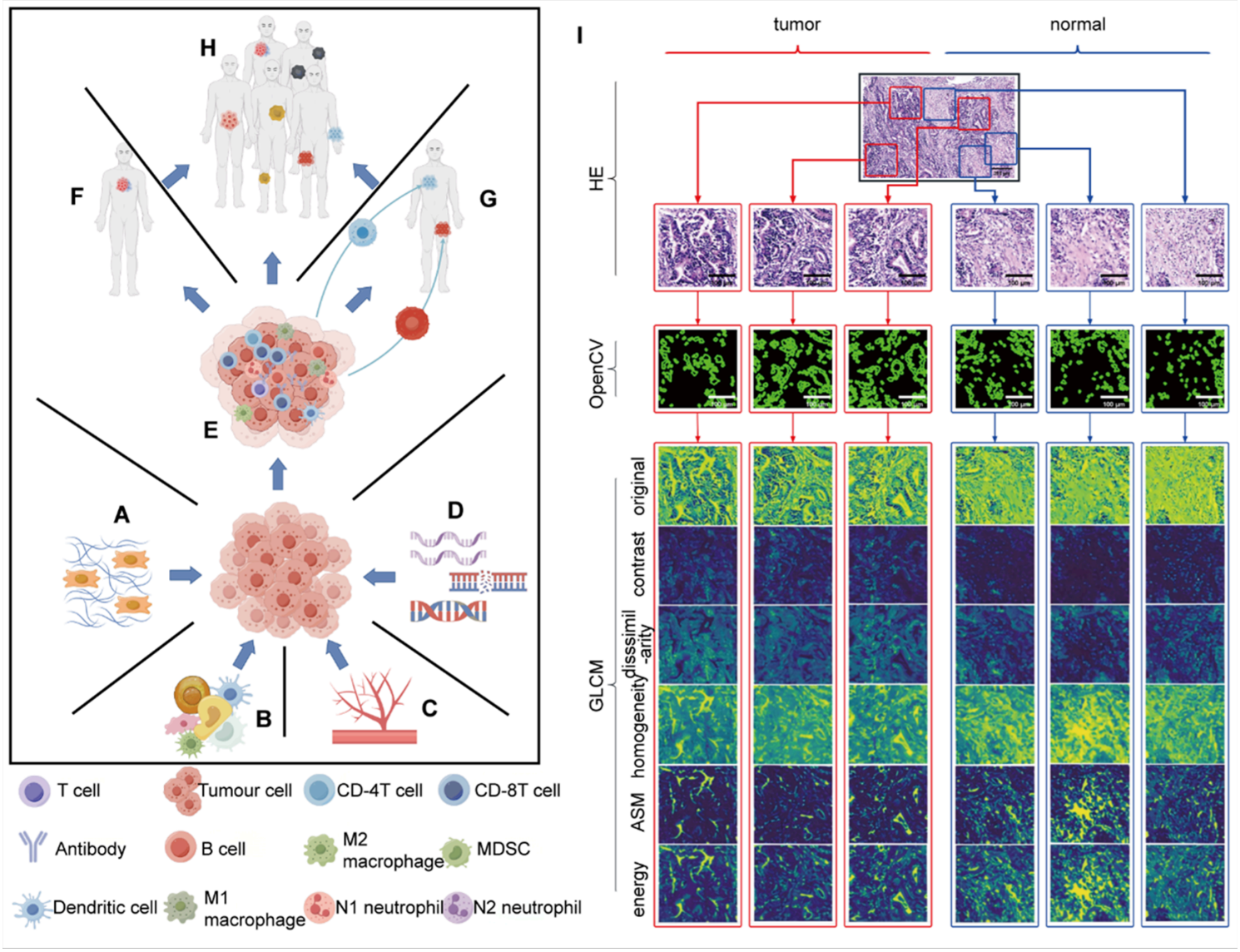


Figure 3

Tumor heterogeneity. (A) Stroma. (B) Immune cells. (C) Nutrients in the microenvironment. (D) Intrinsic factors such as DNA damage and epigenome acting together. (E) and (F) Heterogeneity of primary tumors. (G) Tumor metastasis. (H) Heterogeneity of primary tumors and inter-tumor heterogeneity across populations due to metastasis. (I) Differences in pathological characteristics between tumor cells and non-tumor cells. Scale bar: 100 micrometers.

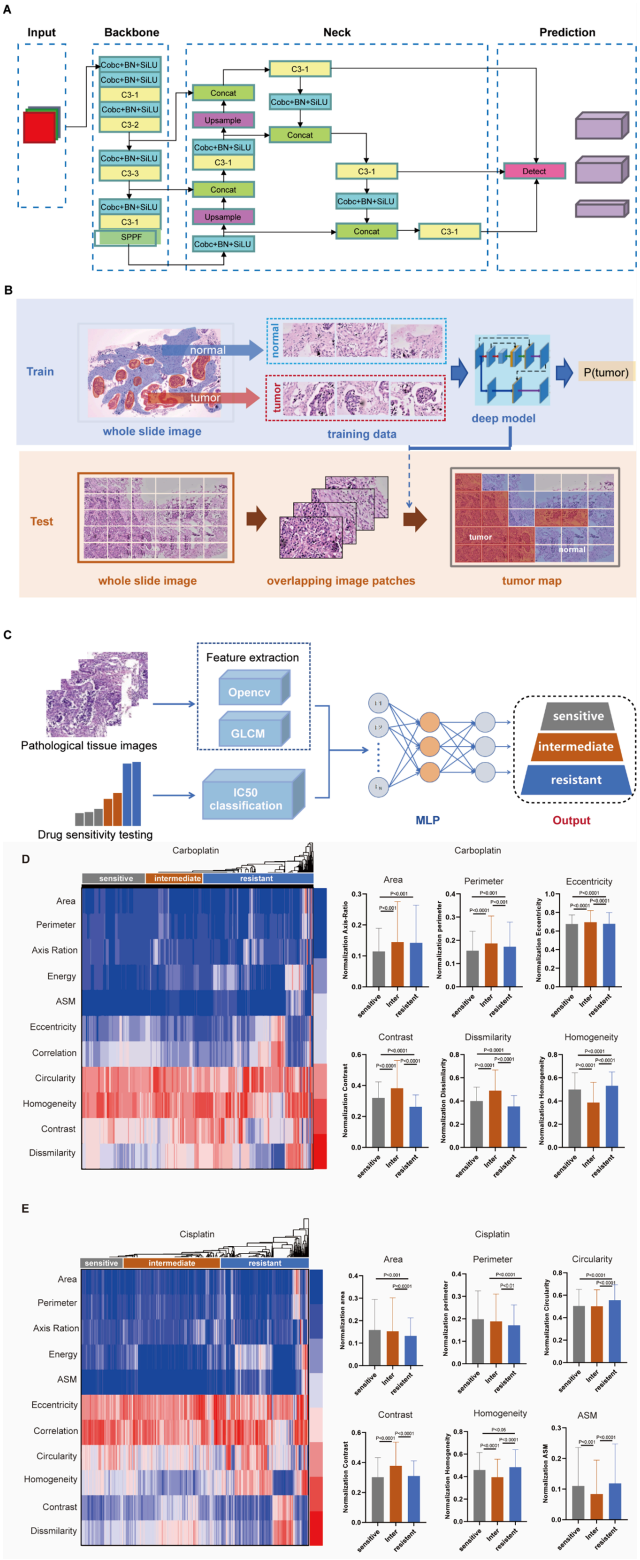


Figure 4

Prediction of sensitivity to platinum-based drugs in breast cancer based on organizational morphology. (A) Schematic diagram of the YOLO-v5 model structure. (B) Deep learning-based tumor region identification framework. (C) Overview of the MLP model prediction process. (D) Correlation between nuclear area and texture features of BC tissue and sensitivity to carboplatin. (E) Correlation between nuclear area and texture features of BC tissue and sensitivity to cisplatin.

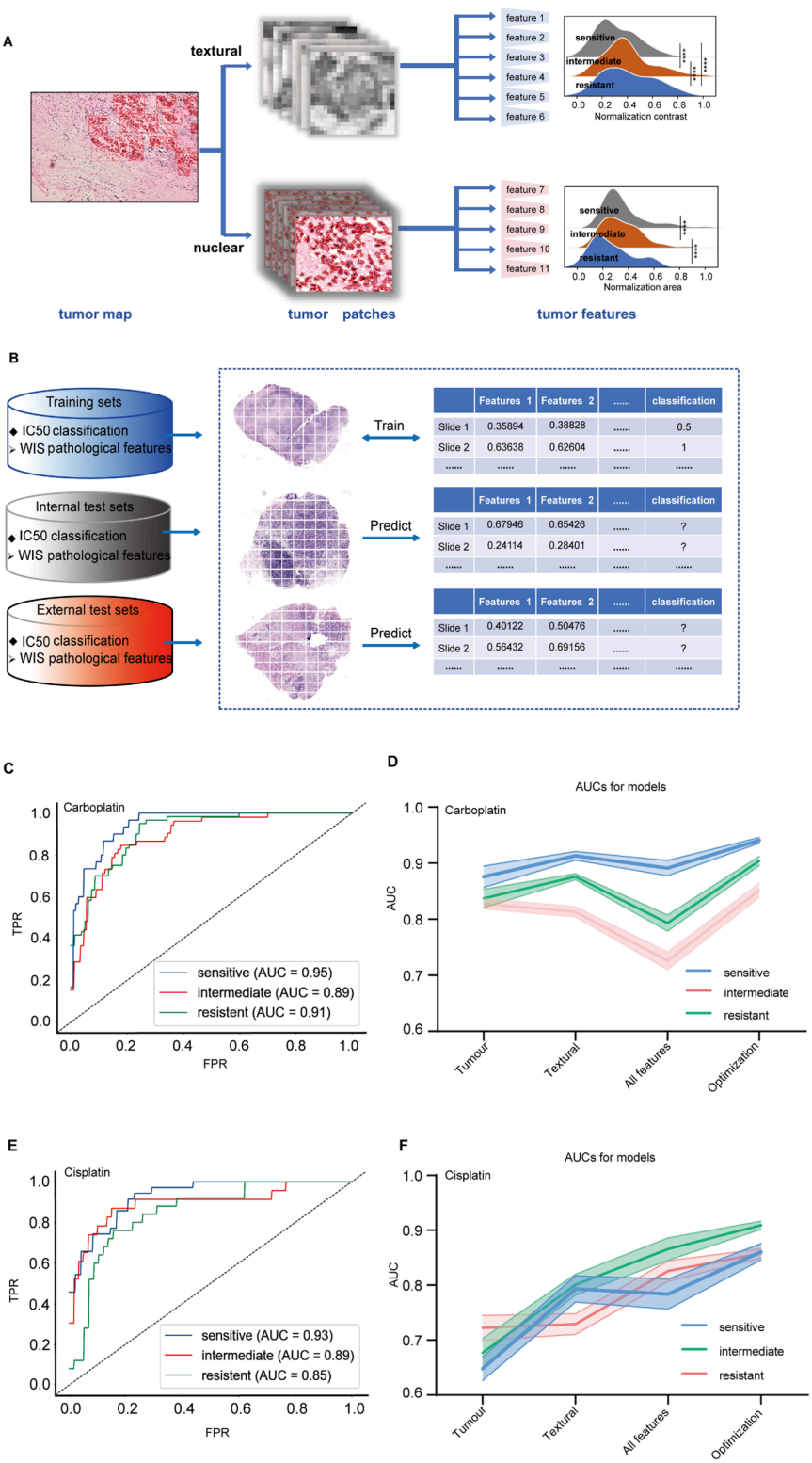


Figure 5

Drug sensitivity prediction model for breast cancer organoids. (A) Tumor region feature extraction framework. (B) MLP model. (C) and (D) ROC curve of the MLP model based on carboplatin drug sensitivity. (E) and (F) ROC curve of the MLP model based on cisplatin drug sensitivity.

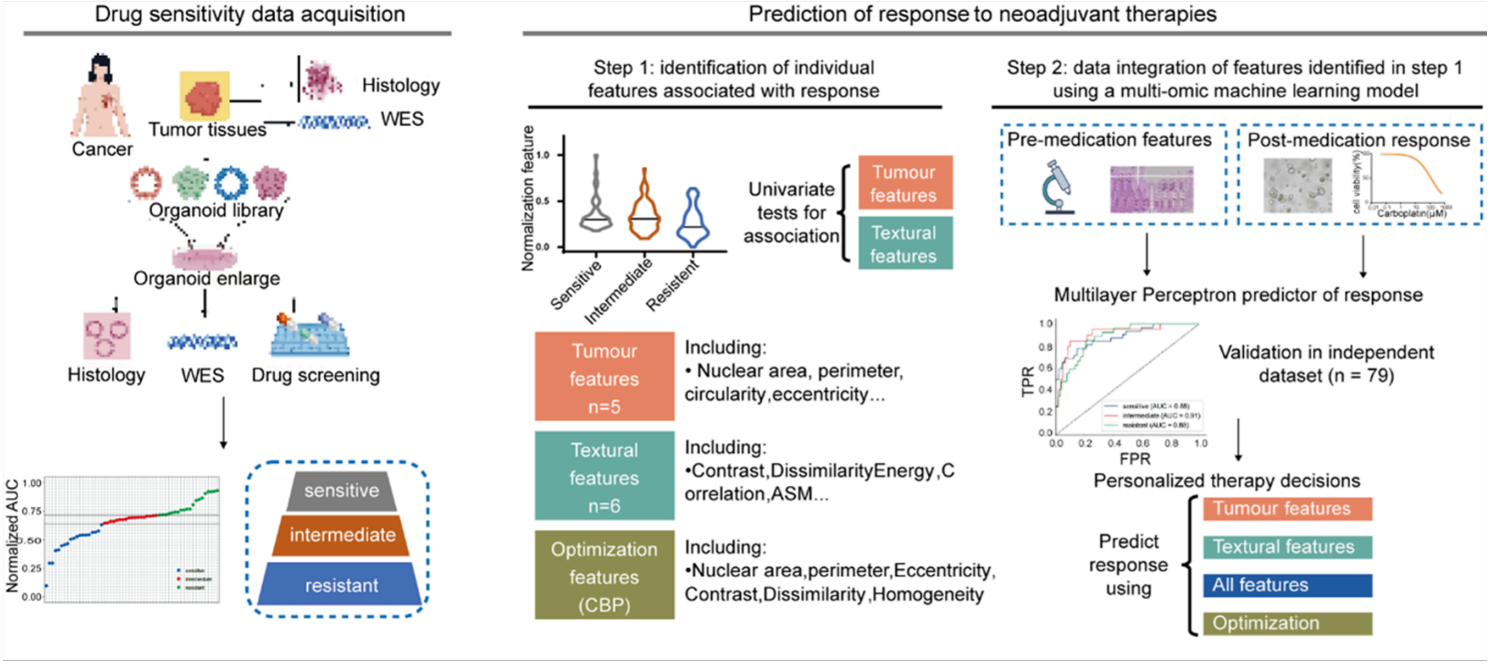


Figure 6

Prediction model for the sensitivity of BC patients to platinum-based drug treatment.

Supplementary Files

This is a list of supplementary files associated with this preprint. Click to download.

- supplymentNPJPRECISIONONCOLOGY.docx